RP Current Trends in Engineering and Technology
Vol. 2, No. 1 (January – March 2023) pp. 32–40
e-ISSN: 2583-5491

RESEARCH PLATEAU PUBLISHERS

Cite this article: J. Singh, Stimulated Raman scattering in weakly polar narrow band gap magnetized semiconductors in the presence of hot carriers, *RP Cur. Tr. Eng. Tech.* **2** (2023) 32–40.

Original Research Article

Stimulated Raman scattering in weakly polar narrow band gap magnetized semiconductors in the presence of hot carriers

Jaivir Singh
Department of Physics, J.V.M.G.R.R. College, Charkhi Dadri - 127306, Haryana, India
*Corresponding author, E-mail: jaivir.bmu@gmail.com

ARTICLE HISTORY
Received: 4 Nov. 2022
Revised: 16 Feb. 2023
Accepted: 18 Feb. 2023
Published online: 20 Feb. 2023

KEYWORDS
Hydrodynamic model; Semiconductor plasmas; Stimulated Raman Scattering (SRS); Threshold pump electric field; Gain coefficient; Optimum pulse duration.

ABSTRACT
By employing the hydrodynamic framework of semiconductor plasmas, an in-depth analytical study has been carried out to explore both the steady-state and transient Raman gain in a weakly polar, narrow band-gap, magnetized single-component semiconductor, namely n-InSb, when subjected to off-resonant laser excitation. Since stimulated Raman scattering (SRS) originates from the third-order (Raman) susceptibility of the medium, expressions have been derived for the threshold pump electric field, the corresponding gain coefficients (in steady and transient regimes), and the optimum pulse duration required for the onset of SRS. The application of a strong external magnetic field is found to reduce the threshold pump field while simultaneously increasing the Raman gain. Moreover, heating of charge carriers by the intense pump beam alters the electron collision frequency, thereby modifying the nonlinear properties of the medium, which in turn leads to a substantial enhancement of the Raman gain. Such an enhancement proves highly beneficial for the compression of scattered pulses. The outcomes of this investigation not only provide deeper insight into the SRS mechanism in both solid-state and gaseous plasmas but also serve to bridge the gap between theoretical predictions and experimental observations.

1. Introduction

Nonlinear optics (NLO) represents a highly significant area of physics and technology, primarily dealing with the interaction between intense laser radiation and matter [1]. Broadly, the phenomena studied under NLO can be classified into two main groups: (i) steady-state (SS) nonlinear optical effects and (ii) coherent transient (TR) optical effects. A wide range of nonlinear processes—including parametric interactions, self-focusing and self-defocusing, stimulated scattering, optical phase conjugation, optical bistability, and their applications in frequency conversion, amplification, and optical signal processing—typically arise under continuous-wave laser operation or when laser pulses have durations much longer than the characteristic dephasing or recombination times of the medium. These are collectively referred to as steady-state nonlinear effects (SS-NLEOs). The physical basis of such effects in crystalline media is often associated with anharmonic lattice potentials, the dynamics of free carriers, and photo-generated charge carriers. In contrast, coherent transient optical effects—such as optical nutation, free induction decay, photon echo, and self-induced transparency—emerge when the incident laser pulse duration is much shorter than the dephasing or recombination time of the resonant excited state. Under these conditions, the medium retains the induced optical coherence for a finite duration, even after the excitation pulse is switched off.

Among the various SS-NLOs, the stimulated scattering of laser light remains one of the most extensively explored areas of research. On the fundamental side, it yields microscopic insights into the mechanisms of laser–matter interaction, while on the applied side, it plays a vital role in advancing modern optical technologies [1, 2]. When a powerful coherent laser beam travels through a medium, it can excite the natural vibrational modes of that medium, such as electron–plasma waves and ion waves. If the excited mode corresponds to a high-frequency vibration, the process manifests as stimulated Raman scattering (SRS) [3–6]. SRS serves as an effective diagnostic tool, enabling the study of vibrational energies, lifetimes, and dephasing mechanisms of the medium. Additionally, it has proven valuable in extending the tunability of coherent optical sources across a broad portion of the infrared spectrum [7, 8]. Through the use of dye lasers, the anti-Stokes component of SRS can also be exploited to generate tunable ultraviolet (UV) radiation [9]. In recent years, four-wave mixing interactions, which arise due to the third-order nonlinear susceptibility, have attracted considerable attention. Under suitable conditions, these interactions can produce nonlinear devices that function in a manner similar to those based on three-wave mixing. A particularly important application of such interactions in modern optics is the generation of optical phase conjugation (OPC) in active media [10]. Furthermore, it is now well established that techniques like coherent anti-Stokes Raman spectroscopy (CARS) and Raman-induced Kerr effect spectroscopy (RIKES) rely on nonlinear four-wave mixing processes for their operation.

Extensive studies have been carried out on Raman scattering and the associated instabilities in gaseous plasmas

[11–13]. However, the practical applications of semiconductors have increasingly attracted the attention of solid-state physicists, particularly in fields such as spectroscopy, laser development, and device fabrication. In the pursuit of optical memories and switching elements, it has been observed that the optical response of semiconductors undergoes significant changes when electrons are excited by light. From an electrical standpoint, semiconductors occupy an intermediate position between metals, which contain nearly free electrons, and insulators, where electrons are tightly bound. This intermediate nature makes them especially valuable as nonlinear materials in both electronics and optics, since their properties can be readily tuned by external fields, material composition, or microstructural modifications. As a result, semiconductors have established themselves as indispensable active media in a wide spectrum of technologies, including laser communication, advanced optoelectronic devices, optical computing [14, 15], and all-optical signal processing [16]. Therefore, gaining a deeper understanding of the mechanisms underlying transient effects in semiconductor crystals is of fundamental importance for both basic science and applied research.

Recent studies on stimulated Raman scattering (SRS) in magnetoactive doped semiconductors show notable gaps between theory and experiment [17–20]. Low-intensity short-pulse experiments suggest SRS occurs below the predicted threshold, while high-intensity studies report signal saturation well below theoretical values. Singh et al. [21] analytically studied SS and TR Raman gain coefficients of weakly-polar magnetoactive doped semiconductors [22] and found strong Raman growth at pump fields of ~10^8 V/m. In semiconductors, intense pump–carrier interaction raises carrier temperature due to high mobility, small effective mass, and slow energy transfer to the lattice. Earlier work linked SRS in polar semiconductors mainly to differential polarizability, but the Szigeti effective charge, crucial in the infrared region [23, 24], must also be included for accurate theoretical models and applications.

A review of existing literature shows that no systematic effort has yet been made to examine the role of carrier heating in the SRS process, where its origin is attributed to the finite Szigeti effective charge and differential polarizability in narrow band-gap magnetized semiconductors. In this work, employing a hydrodynamic model of semiconductor plasma, we investigate how pump-induced carrier heating affects the steady-state and transient Raman gain coefficients.

The motivation for this study arises from the fact that pump-induced carrier heating can significantly alter the medium's nonlinearity and the associated phenomena. With the advent of high-power lasers, such investigations are crucial for improving our understanding of scattering mechanisms in solid and gaseous plasmas, thereby helping bridge the gap between theoretical predictions and experimental results.

The fundamental physical origin of the process can be traced to the non-vanishing nonlinear polarization that develops within the medium. This polarization arises due to the coupling of molecular vibrations, particularly those oscillating at the transverse optical phonon frequency (Ω), with the externally applied pump frequency (Ω_0). In addition, the system also couples with the electron plasma frequency (Ω_p), thereby introducing further complexity into the interaction. The presence of a static magnetic field, characterized by $\Omega_t < \Omega_p < \Omega_0$ and $\Omega_c (< \Omega_0) \gg \Omega_c [= 0.5(\Omega_t^2 + \Omega_p^2)^2]$, plays a crucial role in modifying this coupling. Under these conditions, the combined effects of phonon dynamics, plasma oscillations, and magnetic field influence give rise to a rich variety of nonlinear phenomena, ultimately leading to the manifestation of the process under study.

2. Theoretical formulations

This section presents the theoretical framework for deriving the complex effective third-order (Raman) susceptibility, from which the corresponding steady-state and transient Raman gain coefficients for the Stokes component of the scattered electromagnetic wave in a Raman-active medium are obtained. To this end, we analyze the propagation of a hybrid pump wave, expressed as:

$$\vec{E}_0 = (E_{0x}\hat{i} + E_{0y}\hat{j})\exp[i(k_0 x - \Omega_0 t)] \quad (1)$$

in a homogeneous semiconductor plasma subjected to an external magnetostatic field $\vec{B}_0 = B_{0x}\hat{i} + B_{0z}\hat{k}$. The magnetic field is oriented in the x–z plane, making an angle θ with the x-axis, as illustrated schematically in Figure 1.

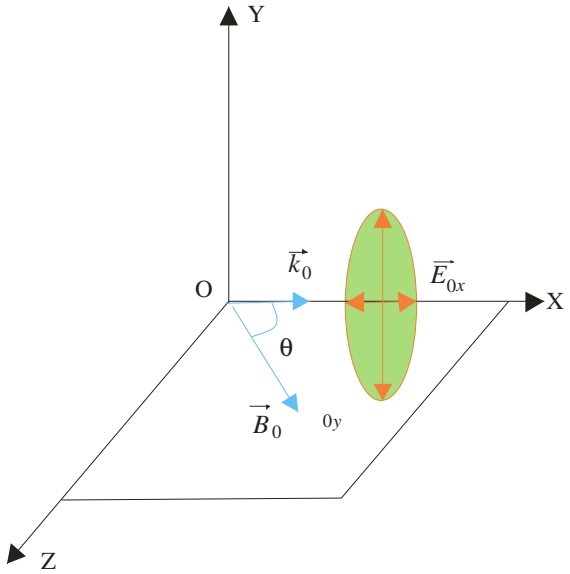

Figure 1: Schematic representation of the geometry of stimulated Raman scattering (SRS) in the presence of an external magnetic field.

The present field geometry has been selected because, in most previously reported studies, the pump wave is assumed to propagate exactly parallel to the applied magnetic field. However, such a condition is often experimentally impractical. In addition, earlier models generally considered the pump electric field to be oriented either strictly parallel or strictly perpendicular to the direction of propagation, which again does not reflect realistic physical situations [25]. For a finite solid-state plasma, the pump field must inherently possess components both along and perpendicular to the propagation direction. Therefore, the most realistic scenario—adopted in this work—is to analyze a hybrid mode that propagates obliquely with respect to the external magnetic field.

In a Raman-active medium, the scattering of a high-frequency pump wave is significantly enhanced through the excitation of a normal vibrational mode (optical phonon). For theoretical treatment, the Raman medium is modeled as containing N harmonic oscillators per unit volume, with each oscillator described by its displacement coordinate (x), molecular mass (M), and normal vibrational coordinate u (x, t).

The equation of motion describing a single oscillator, representing an optical phonon, can be expressed as follows [26]:

$$\frac{\partial^2 u}{\partial t^2}+\gamma\frac{\partial u}{\partial t}+\Omega_\eta^2 u=\frac{(F_q+F_\alpha)}{M} \tag{2}$$

Here, γ denotes the damping constant, which is equal to the phenomenological phonon–collision frequency ($\sim 10^{-2}\Omega_\eta$) [27]. The parameter Ω_η represents the un-damped molecular vibrational frequency, taken to be equal to the transverse optical phonon frequency.

$F_Q(=qE)$ and $F_\alpha(=(1/2)\varepsilon(\Delta\alpha)\bar{E}^2)$ correspond to the driving force per unit volume acting on the medium forces arising from the Szigeti effective charge (q) and the differential polarizability ($\Delta\alpha$), respectively. The overbar notation on E indicates an average over several optical cycles, since the molecular system cannot directly respond to rapid oscillations at optical frequencies. Furthermore, $\varepsilon = \varepsilon_0\varepsilon_\infty$, where ε_0 and ε_∞ denote the static permittivity and the high-frequency permittivity of the medium, respectively.

The fundamental set of equations employed in the present analysis are as follows:

$$\frac{\partial\vec{v}_0}{\partial t}+\nu\vec{v}_0=\frac{e}{m}[\vec{E}_0+(\vec{v}_0\times\vec{B}_0)]=\frac{e}{m}\vec{E}_e \tag{3}$$

$$\frac{\partial\vec{v}_1}{\partial t}+\nu\vec{v}_1+\left(\vec{v}_0.\frac{\partial}{\partial x}\right)\vec{v}_1=\frac{e}{m}[\vec{E}_1+(\vec{v}_1\times\vec{B}_1)] \tag{4}$$

$$\frac{\partial n_1}{\partial t}+n_e\frac{\partial v_1}{\partial x}+n_1\frac{\partial v_0}{\partial x}+v_0\frac{\partial n_1}{\partial x}=0 \tag{5}$$

$$\vec{P}_{mv}=\varepsilon N(\Delta\alpha)u^*\vec{E}_e \tag{6}$$

$$\frac{\partial E_{1x}}{\partial x}=-\frac{n_1 e}{\varepsilon}-\frac{1}{\varepsilon}\frac{\partial P_{mv}}{\partial x} \tag{7}$$

Equations (3) and (4) describe the rate equations for the pump and signal beams, respectively, in the presence of a magnetostatic field. Here, $\vec{B}_0$ and $\vec{B}_1$ represent the equilibrium and perturbed magnetic fields, while $\vec{v}_0$ and $\vec{v}_1$ denote the oscillatory fluid velocities of the electrons having effective mass m and charge e. The parameter ν corresponds to the electron collision frequency. In Eq. (3), the term $\vec{E}_e$ denotes the effective electric field, which incorporates the Lorentz force contribution ($\vec{v}_0\times\vec{B}_0$) from the external magnetic field and is expressed explicitly as $\vec{E}_e=\vec{E}_0+(\vec{v}_0\times\vec{B}_0)$. The electron continuity equation, given by Eq. (5), involves the equilibrium and perturbed carrier concentrations, n_e and n_1, respectively. Equation (6) defines the nonlinear polarization $\vec{P}_{mv}$ that arises from the natural vibrational modes driven by the applied electric field. The space-charge field $\vec{E}_1$ is obtained using Poisson's equation (Eq. (7)), where the second term accounts for the differential polarizability of the medium. Molecular vibrations at frequency Ω cause a modulation of the dielectric constant, which leads to an exchange of energy between electromagnetic fields differing in frequency by integral multiples of Ω, i.e., $\Omega_0 \pm p\Omega$, where p = 1, 2, 3, … Modes with frequency ($\Omega_0 + p\Omega$) are referred to as anti-Stokes modes, while those at ($\Omega_0 - p\Omega$) are the Stokes modes. Since the present analysis focuses only on the first-order Stokes component of the scattered electromagnetic wave, the energy and momentum conservation (phase-matching) conditions to be satisfied are: $\hbar\Omega_s=\hbar\Omega_0-\hbar\Omega$ and $\hbar\vec{k}_s=\hbar\vec{k}_0-\hbar\vec{k}$.

2.1 Induced current density

The high-frequency pump field produces a carrier density perturbation, which in turn excites an electron–plasma wave and induces a current density in the Raman-active medium. Following the standard theoretical approach developed by Sen and Sen [17], the perturbed electron density (n_1) of the Raman-active medium, arising from molecular vibrations, can be derived from Eqs. (2)–(7) as:

$$n_1=i\frac{\varepsilon k}{e}\left[\frac{(\Omega_\eta^2-\Omega^2+i\gamma\Omega)-\left(\frac{\varepsilon N}{2M}\right)q_\alpha}{\left(\frac{\varepsilon}{2M}\right)(\Delta\alpha)(E_e)_x^*}\right]u^*. \tag{8}$$

where $q_\alpha=\frac{2q_s(\Delta\alpha)}{\varepsilon}-(\Delta\alpha)^2\left|(E_e)_x\right|^2$.

The density perturbation arising from molecular vibrations at frequency Ω interacts (beats) with the pump field at frequency Ω_0, generating high-frequency components of the density modulation. The Stokes component of this perturbed density, occurring at frequency Ω_s, can be expressed as:

$$n_s=\frac{ie(k_0-k)(E_e)_x}{m(\Delta_1^2-i\nu\Omega_s)}n_1^*, \tag{9}$$

where $\Delta_1^2=\bar{\Omega}_r^2-\Omega_s^2$ and suffixes t and s denote the components of the perturbed carrier concentration associated with normal vibrations in the medium and the first-order Stoke's mode respectively. In Eq. (9)

$$\bar{\Omega}_r^2=\Omega_r^2\left[\frac{\Omega_{cx}^2+\nu^2}{\Omega_c^2+\nu^2}\right], \text{ in which } \Omega_r^2=\frac{\Omega_p^2\Omega_\eta^2}{\Omega_\eta^2},$$

$$\Omega_{cx,z}\left(=\frac{eB_{sx,z}}{m}\right),\ \Omega_p=\left(\frac{n_e e^2}{m\varepsilon_0\varepsilon_L}\right)^{1/2}, \text{ and } \frac{\Omega_\eta}{\Omega_\eta}=\left(\frac{\varepsilon_L}{\varepsilon_\infty}\right)^{1/2}.$$

Ω_η is the longitudinal optical phonon frequency, given by $\Omega_\eta=k_B\Theta_D/\hbar$, where k_B is the Boltzmann constant and Θ_D is the Debye temperature of the lattice. ε_L represents the lattice dielectric constant.

The components of the oscillatory electron fluid velocity in the presence of the pump and magnetostatic fields can be determined from Eq. (3) as:

$$v_{0x} = \frac{\bar{E}}{\nu - i\Omega_0}, \tag{10a}$$

$$v_{0y} = \frac{eE_{0x}}{m}.\frac{[\Omega_{cz} + (\nu - i\Omega_0)]}{[\Omega_{cz}^2 + (\nu - i\Omega_0)^2]}. \tag{10b}$$

The resonant Stokes component of the current density, arising from the finite nonlinear polarization of the medium, can be obtained by neglecting the transient dipole moment and is expressed as:

$$\vec{J}_{cd}(\Omega_s) = n_e e\vec{v}_{1x} + n_s^* e\vec{v}_{0x}, \tag{11}$$

which yields

$$\vec{J}_{cd}(\Omega_s) = \frac{\varepsilon\Omega_p^2 E_{1x}}{(\nu - i\Omega_s)} + \frac{\varepsilon k(k_0 - k)Z_1 \left|\bar{E}_0\right|^2 E_{1x}}{(\Delta_1^2 + i\nu\Omega_s)(\nu - i\Omega_s)}, \tag{12}$$

where $\Delta_2^2 = \bar{\Omega}_r^2 - \Omega^2$, and $Z_1 = 1 - \frac{\varepsilon N}{2M}\frac{q_\alpha}{(\Delta_2^2 + i\gamma\Omega)}$.

In Eq. (12), the first term corresponds to the linear component of the induced current density, whereas the second term accounts for the nonlinear coupling between the three interacting waves through the nonlinear current density.

2.2 Threshold pump amplitude and optical susceptibilities

To start, the induced polarization $\vec{P}_{cd}(\Omega_s)$ can be expressed as the time integral of the current density $\vec{J}_{cd}(\Omega_s)$, which leads to:

$$\vec{P}_{cd}(\Omega_s) = \int \vec{J}_{cd}(\Omega_s)dt. \tag{13}$$

Following the method of Singh et al. [28], the nonlinear induced polarization is obtained from the perturbed current density.

$$\vec{P}_{cd}(\Omega_s) = \frac{e^2\varepsilon_\infty k(k_0 - k)Z_1 \left|\bar{E}_0\right|^2 \vec{E}_{1x}}{m^2\Omega_0\Omega_s(\Delta_1^2 + i\nu\Omega_s)}. \tag{14}$$

From the above relation, the threshold for the onset of the SRS process can be determined by setting $P_{cd}(\Omega_s) = 0$. This leads to:

$$E_{th} = \frac{m}{ek}\frac{\Delta_1\Delta_2(\Omega_0^2 - \Omega_c^2)}{[(\Omega_0^2 - \Omega_{cx}^2) + \nu\Omega_{cz}]}. \tag{15}$$

This equation indicates that E_{th} is strongly dependent on the material properties (n_e, v), the applied magnetic field (B_0), and the geometry (θ) of the field.

In addition to the polarization $\vec{P}_{cd}(\Omega_s)$, the system also exhibits a polarization induced by the interaction of the pump wave with molecular vibrations within the medium, which can be derived from Eqs. (2) and (6) as:

$$\vec{P}_{mv}(\Omega_s) = \frac{\varepsilon^2 N\omega_0^2(\Delta\alpha)^2 \left|E_0\right|^2 \vec{E}_{1x}}{2M(\Delta_2^2 + i\gamma\Omega)}. \tag{16}$$

Therefore, the total polarization induced at the Stokes component, for a pump amplitude well above the threshold, is expressed as:

$$\vec{P}(\Omega_s) = \vec{P}_{mv}(\Omega_s) + \vec{P}_{cd}(\Omega_s) = \left[\frac{\varepsilon^2 N\Omega_0^2(\Delta\alpha)^2}{2M(\Delta_2^2 + i\gamma\Omega)} + \frac{e^2\varepsilon_\infty k(k_0 - k)Z_1}{m^2\Omega_0\Omega_s(\Delta_1^2 + i\nu\Omega_s)}\right]\left|E_0\right|^2 \vec{E}_{1x}. \tag{17}$$

It is well established that the origin of the SRS process resides in the component of $\vec{P}(\Omega_1)$ that depends on $\left|\vec{E}_0\right|^2 \vec{E}_{1x}$. The corresponding effective third-order susceptibility, also referred to as the Raman susceptibility $\chi_R^{(3)}$, is given by:

$$\chi_R^{(3)} = \chi_{mv}^{(3)} + \chi_{cd}^{(3)} = \frac{\varepsilon^2 N\Omega_0^2(\Delta\alpha)^2}{2M(\Delta_2^2 + i\gamma\Omega)} + \frac{e^2\varepsilon_\infty k(k_0 - k)Z_1}{m^2\Omega_0\Omega_s(\Delta_1^2 + i\nu\Omega_s)} \tag{18}$$

Here, ϕ denotes the scattering angle between $\vec{k}_s$ and $\vec{k}_0$. It is evident from Eq. (18) that $\chi_R^{(3)}$ is strongly influenced by both the scattering angle ϕ and the material parameters.

2.3 Carrier heating and modified nonlinearity

To initiate stimulated Raman scattering (SRS), the pump field must exceed the threshold value. When this high-intensity pump propagates through a high-mobility semiconductor, the charge carriers (electrons) absorb energy and momentum from the field, leading to an electron temperature (T_e) that is higher than the lattice temperature (T_0). This field-induced rise in electron temperature subsequently modifies the electron collision frequency (ECF), which can be expressed as [29]:

$$\nu = \nu_0\left(\frac{T_e}{T_0}\right)^{1/2} \tag{19}$$

Here, ν_0 represents the electron collision frequency (ECF) in the absence of the pump, i.e., at $T_e = T_0$. The temperature ratio T_e/T_0 can be determined using the energy balance equation. The power absorbed per electron from the pump field is given by [30]:

$$\frac{e}{2}\mathrm{Re}\left[\vec{v}_{0x}.\vec{E}_e^*\right]=\frac{e^2\nu}{2m}\frac{(\Omega_0^2+\Omega_c^2)}{[(\Omega_0^2+\Omega_c^2)+4\nu^2\Omega_0^2]}\left|\vec{E}_0\right|^2, \tag{20}$$

In the above expression, the asterisk (*) denotes the complex conjugate, while Re indicates the real part of the corresponding quantity. The x-component of $\vec{v}_0$ used in this relation can be evaluated from Eq. (10a).

Following Conwell [31], the power dissipated per electron due to collisions with polar optical phonons (POP) can be expressed as:

$$\left(\frac{\partial\in}{\partial t}\right)_{diss}=\left(\frac{2k_B\theta_D}{m\pi}\right)^{1/2}eE_{PO}(x_e)^{1/2}K_0\left(\frac{x_e}{2}\right).\exp\left(\frac{x_e}{2}\right).\frac{\exp(x_0-x_e)-1}{\exp(x_0)-1} \tag{21}$$

where $x_{0,e}=\dfrac{\hbar\omega_l}{k_BT_{0,e}}$, $\vec{E}_{PO}=\dfrac{me\hbar\Omega_l}{\hbar^2}\left(\dfrac{1}{\varepsilon_\infty}-\dfrac{1}{\varepsilon}\right)$,

Here, $\hbar\Omega_l$ denotes the energy of the polar optical phonon (POP), with θ_D being the Debye temperature of the crystal. The parameters ε and ε_∞ represent the static and high-frequency dielectric permittivities of the medium, respectively, while $K_0(x_e/2)$ is the zeroth-order Bessel function of the first kind.

In the steady-state, the power absorbed per electron from the pump is equal to the power lost due to collisions with POP. For moderate carrier heating, Eqs. (19) and (20) lead to:

$$\frac{T_e}{T_0}=1+\alpha\left|\vec{E}_0\right|^2. \tag{22}$$

where $\alpha=\dfrac{e^2\nu_0\tau}{2m\Omega_0^2}$ (23a)

in which

$$\tau^{-1}=\left(\frac{2k_B\theta_D}{m\pi}\right)^{1/2}eE_{PO}K_0\left(\frac{x_0}{2}\right)\frac{x_0^{1/2}\exp(x_0/2)}{\exp(x_0)-1}. \tag{23b}$$

Thus, the modified electron collision frequency (ECF) can be expressed as:

$$\nu=\nu_0\left(1+\alpha\left|\vec{E}_0\right|^2\right)^{1/2}\approx\nu_0\left(1+\frac{1}{2}\alpha\left|\vec{E}_0\right|^2\right) \tag{24}$$

By substituting this modified electron collision frequency (ECF) into Eq. (18), the effect of carrier heating on the third-order (Raman) susceptibility can be analyzed.

2.4 Steady-state and transient Raman gain coefficients of Stokes component

The steady-state Raman gain coefficient for the Stokes component, under a pump field well above the threshold, is given by:

$$G_R=-\frac{\Omega_s}{\eta c_0}\left[\chi_R^{(3)}\right]_i\left|\vec{E}_0\right|^2=\frac{\varepsilon_\infty\Omega_s\Omega_0^2E_0^2}{2m^2\eta c_0(\Omega_0^2-\Omega\omega_c^2)}\frac{\left[\Omega m^2(\varepsilon N/2M)q_\alpha(\Omega_0^2-\Omega_c^2)(\Delta_2^4+\nu^2\Omega_s^2)-e^2k^2\nu\Omega_0(\Delta_1^4+\gamma^2\Omega^2)\right]}{\left[(\Delta_1^2\Delta_2^2-\nu\gamma\Omega\Omega_s)^2+(\nu\Omega_s\Delta_1^2+\gamma\Omega\Delta_2^2)^2\right]} \tag{25}$$

Equation (25) shows that Raman gain increases quadratically with the pump electric field. In practice, however, the pump field cannot be increased indefinitely, as excessive intensity may damage the sample. Mayer et al. [32] noted that irradiation of a semiconductor with intense, long-duration laser pulses often results in significant heating of the material.

For instance, a typical pump field strength of $E_{0c}\approx10^7$ Vm^{-1} from a Q-switched CO_2 laser with a 170 ns pulse at 10.6 μm wavelength is sufficient to damage InSb at 300 K [33].

It is worth noting that for $E_0 \ll E_{0c}$, the first term of the parameter in Eq. (25) dominates over the second, and the Raman gain arises from the finite Szigeti effective charge and differential polarizability. However, for $E_0 \gg E_{0c}$, the contribution from the effective charge vanishes ($q_s \to 0$), and the Raman gain spectrum depends solely on the differential polarizability.

This scenario ($q_s \to 0$) aligns with the theoretical framework developed by Singh et al. [21]. Accordingly, the present formulation supersedes the traditional approach of relying on high-power pump fields to achieve a large steady-state Raman gain in narrow band-gap magnetoactive semiconductors.

It is evident that the above formulations are limited, both in predicting the optimum pulse durations required to observe Raman gain and in estimating the threshold pump intensity for the onset of Raman instability. This highlights the need to treat SRS by including transient effects. In general, the transient Raman gain coefficient (g_{TR}) is related to the steady-state gain coefficient (g_R) through [34]:

$$G_{TR}=[2G_Rx\Gamma_R\tau_p]^{1/2}-\Gamma_R\tau_p \tag{26}$$

Here, Γ_R denotes the optical phonon lifetime, x is the interaction length, and τ_p is the pulse duration. For backward SRS with very short pump pulses ($\tau_p \le 10^{-10}$ s), the interaction length should be replaced by $c_L\tau_p/2$, where $c_L(=c_0\sqrt{\varepsilon_L})$ is the group velocity of light in the crystal lattice.

Consequently, by setting $G_{TR}=0$ in Eq. (26), the threshold pump intensity for the onset of transient SRS can be expressed as:

$$I_T = \frac{\Gamma_R}{2G_{RR}c_L}, \tag{27}$$

Here, $G_{RR} = G_R / I_p$ is the steady-state Raman gain coefficient per unit pump intensity, and $I_0 = (1/2)\eta\varepsilon_0 c\left|\vec{E}_0\right|^2$.

For comparatively long pulse durations ($\tau_p \geq 10^{-9}$ s), the cell length can be taken as x. Under these conditions, we find:

$$G_{TR} = (\Gamma_R\tau_p)^{1/2}[-(\Gamma_R\tau_p)^{1/2} + (G_R x)^{1/2}]. \tag{28}$$

The above expression provides an estimate of the optimum pulse duration $\tau_{p,opt}$, above which no transient gain can be achieved. By setting $G_{TR} = 0$, this condition yields:

$$\tau_{p,opt} \approx \frac{G_R}{\Gamma_R}. \tag{29}$$

The calculated values of $\tau_{p,opt}$ indicate that the optimum pulse duration can be increased by raising the pump intensity. Equation (29) explains the suppression of Raman gain at large pulse durations.

3. Results and discussion

To verify the accuracy of the current model and to investigate the stimulated Raman scattering (SRS) process, we consider a weakly polar, narrow band-gap semiconductor crystal (n-InSb) at a temperature of 77 K as the medium. This crystal is assumed to be exposed to a 10.6 μm CO_2 laser with frequency $\Omega_0 = 1.78\times10^{14}$ s^{-1}. The physical parameters used are adopted from References [17-21].

Based on the material parameters described earlier, we examine how the threshold pump amplitude E_T varies with the magnetic field strength B_0 in the InSb crystal, considering the magnetic field inclination θ as a parameter. The results are illustrated in Figure 2.

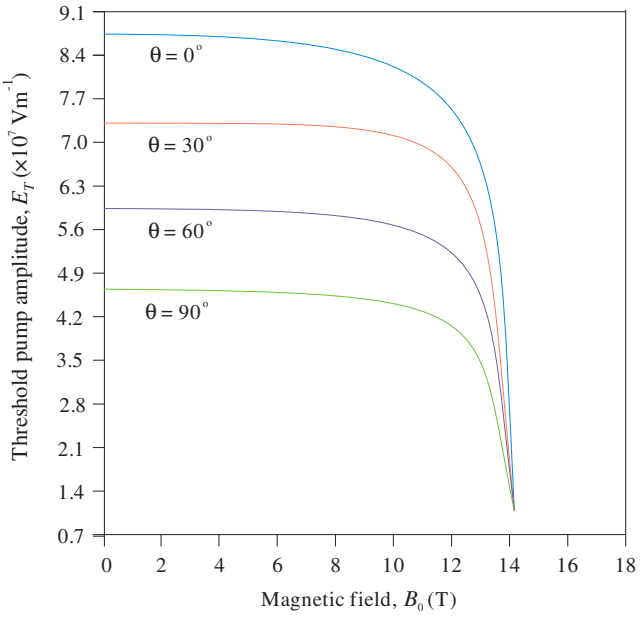

Figure 2: Variation of the threshold pump amplitude E_T with magnetic field strength B_0) for different values of θ. The parameters used are $n_e = 2\times10^{22}$ m^{-3} and $\phi = 30^o$.

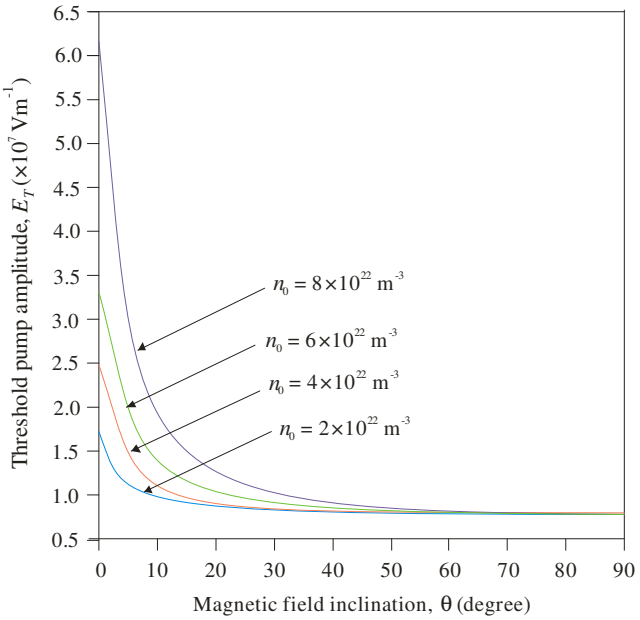

Figure 3: Variation of the threshold pump amplitude E_T with magnetic field inclination θ for different values of n_e. The parameters used are $B_0 = 14$ T and $\phi = 30^o$.

In all cases, initially E_T has a high value at $B_0 = 0$ T, remains nearly constant up to $B_0 = 10$ T, and then decreases sharply as B_0 increases further. For strong magnetic fields, E_T becomes independent of θ, causing the curves to overlap.

Figure 3 shows the variation of E_T with the magnetic field inclination θ. In the case of a longitudinal magnetic field, a heavily doped medium requires a threshold field that is an order of magnitude higher than that of a moderately doped medium. However, as θ increases, E_T decreases, and the difference between the curves becomes smaller. For $\theta \to 90^o$, the two curves converge, indicating that the magnetic field renders independent of the carrier concentration.

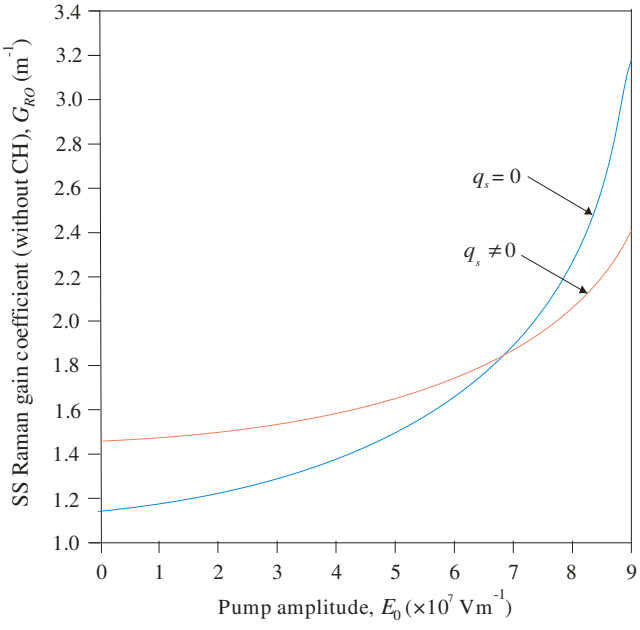

Figure 4: (a) Dependence of the steady-state Raman gain coefficient G_{RO} (without considering carrier heating) on the pump field strength E_0 for $q_s = 0$ (curve (a)) and $q_s \neq 0$ (curve (b)).

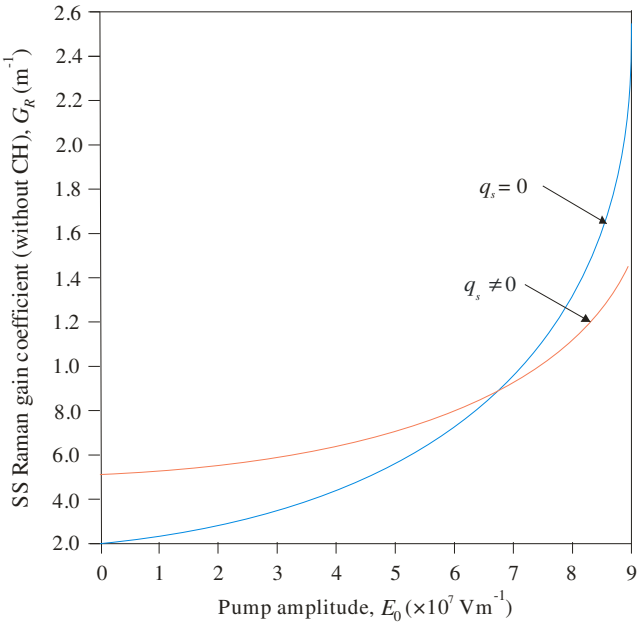

Figure 4: (b) Dependence of the steady-state Raman gain coefficient G_R (considering carrier heating) on the pump field strength E_0 for $q_s = 0$ (curve (a)) and $q_s \neq 0$ (curve (b)). The parameters used are $n_e = 2\times10^{22}$ m^{-3}, $B_0 = 14$ T, $\phi = 30^o$, $\theta = 60^o$.

A key goal of this study is to examine how steady-state Raman gain coefficients—both without carrier heating and with carrier heating—depend on the pump field strength, as illustrated for curve (a) and curve (b) in Figs. 4(a) and 4(b), respectively. In both scenarios, the Raman gain increases with the input pump field strength [Eq. 25]. Notably, for lower pump field strengths, the Szigeti effective charge contributes more significantly than the differential polarizability. Conversely, at higher pump field strengths $E_0 < E_c (= 6.8\times10^7\ \text{Vm}^{-1})$, the Raman gain is primarily governed by differential polarizability. This occurs because, at these higher field strengths, the second term in Eq. (25) becomes dominant, effectively diminishing the contribution of the Szigeti effective charge. At a specific intermediate pump field strength $E_0 = E_c$, both the Szigeti effective charge and the differential polarizability contribute equally to the steady-state Raman coefficients. However, at higher pump field strengths $E_0 > E_c$, the Raman gain arises mainly from differential polarizability. This happens because, at such field strengths, the second term in Eq. (25) becomes dominant, effectively suppressing the contribution from the Szigeti effective charge. Therefore, including the Szigeti effective charge in the analysis provides an alternative to the conventional approach of relying on high pump field strengths to achieve substantial steady-state Raman gain.

A comparison of Figures 4(a) and 4(b) reveals a notable observation: the steady-state Raman gain coefficient in the presence of carrier heating is approximately 4.33 times larger than that without carrier heating. This significant enhancement can be attributed to the increase in the effective coupling factor (ECF) [Eq. (24)] caused by carrier heating. The rise in ECF leads to greater energy transfer between the pump and Stokes modes, which in turn amplifies the steady-state Raman gain.

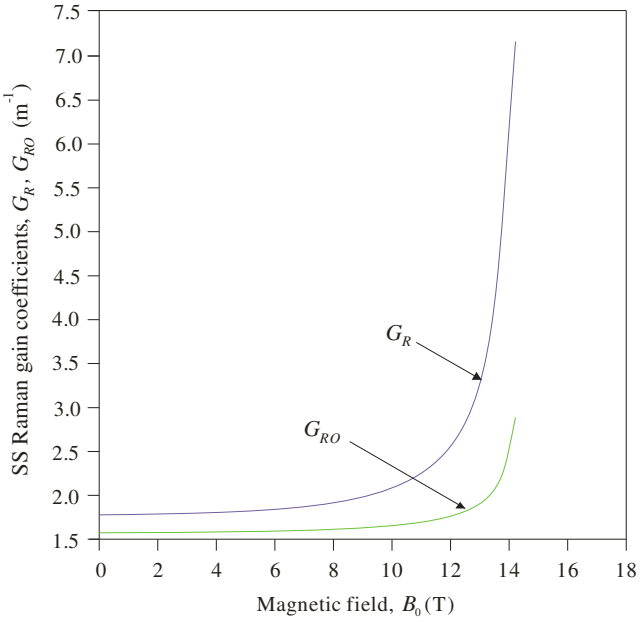

Figure 5: Dependence of the steady-state Raman gain coefficients, G_R and G_{RO}, on the magnetic field strength B_0). The parameters used are $E_0 = 6.8\times10^7\ \text{Vm}^{-1}$, $n_e = 2\times10^{22}$ m^{-3}, $\phi = 30^o$, $\theta = 60^o$.

Figure 5 shows the variation of steady-state Raman gain coefficients, g_R and g_{RO} with magnetic field strength. A notable feature in this figure is that both gain coefficients remain almost constant at lower magnetic fields. However, at $B_0 = 12$ T the gain coefficients increase sharply. Consequently, a maximum steady-state Raman gain is achieved at $B_0 = 14.2$ T ($\Omega_c \sim \Omega_0$), which becomes effectively independent of the magnetic field. This suggests that the stimulated laser can be tuned by adjusting the magnetic field (cyclotron frequency) near the pump frequency, consistent with the findings reported by my research group in earlier works [18-22] for steady-state gain coefficients.

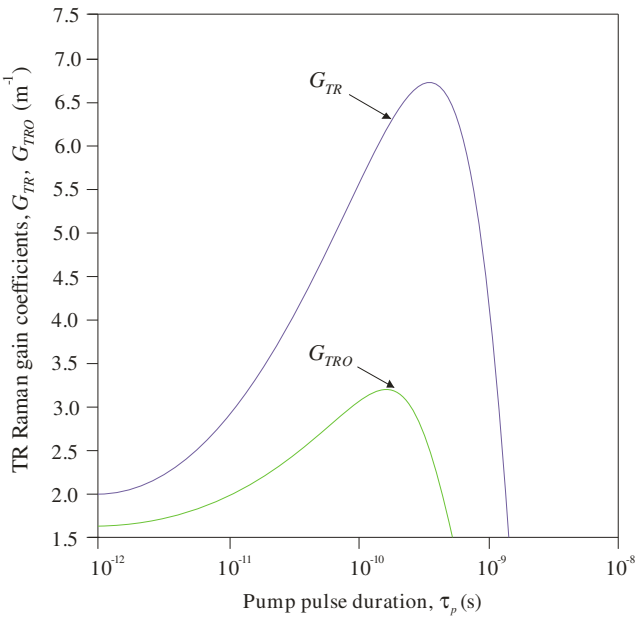

Figure 6: Dependence of transient Raman gain coefficients, G_{TR} and G_{TRO} on the pump pulse duration, τ_p. The parameters used are $I_0 = 1.8\times10^{12}\ \text{Wm}^{-2}$, $n_e = 2\times10^{22}$ m^{-3}, $B_0 = 14$ T, $\phi = 30^o$, $\theta = 60^o$.

Figure 6 illustrates the effect of pump pulse duration, τ_p, on the transient Raman gain of the Stokes mode. Here, G_{TR} and G_{TRO} represent the transient Raman gain coefficients with and without the inclusion of carrier heating by the pump, respectively. To generate this behavior, pulse durations in the range $10^{-12} \le \tau_p \le 10^{-8}$ s and a pump field intensity $I_0 \approx 5\times10^{12}\,\mathrm{Wm}^{-2}$ were considered, with the interaction length taken as the cell length, *x*. The gain coefficients increase with pulse duration, reaching a maximum at a specific value, after which they remain nearly constant over a certain range of pulse duration. These regions can be identified as quasi-steady states or quasi-saturation regimes. The presence of carrier heating not only enhances the transient Raman gain coefficient but also shifts the gain saturation regime toward higher values. This enhancement in can be attributed to an increase in the effective coupling factor (ECF), which promotes greater energy transfer between the pump and Stokes modes, thereby increasing g_{TR}. If τ_p exceeds the quasi-saturation range, the transient gain coefficients decrease rapidly. This behavior aligns closely with experimental observations in CS_2 [35], where the saturation of Raman conversion efficiency—proportional to the exponential of the gain factor—drops significantly at longer pulse durations. Hence, incorporating carrier heating in the analysis not only renders the model more realistic and the results more reliable but also helps minimize discrepancies between theoretical predictions and experimental observations.

4. Conclusions

The present study presents an analytical investigation of steady-state and transient Raman gain in weakly polar, narrow band-gap magnetized semiconductors irradiated by a pulsed 10.6 μm CO_2 laser. The effect of carrier heating induced by the pump has been examined in detail. Carrier heating significantly enhances the effective collision frequency (ECF), facilitating greater energy transfer from the pump to the scattered light. Consequently, both steady-state and transient Raman gain coefficients are substantially increased. Incorporating carrier heating in the analysis may therefore help reduce discrepancies between theoretical predictions and experimental measurements, providing a more accurate interpretation of observations in solid and gaseous plasmas.

The application of a strong transverse magnetic field further lowers the threshold pump field required for the onset of stimulated Raman scattering (SRS) and enhances both steady-state and transient Raman gain coefficients in weakly polar semiconductors. For lower pump field strengths $E_0 < E_c$, the contribution of the Szigeti effective charge dominates over differential polarizability. At higher pump field strengths $E_0 > E_c$, however, Raman gain is primarily governed by differential polarizability. At a particular intermediate pump field strength $E_0 = E_c$, both Szigeti effective charge and differential polarizability contribute equally to the steady-state Raman coefficients. Including the Szigeti effective charge in the analysis provides an alternative to the conventional approach of using high pump field strengths to achieve significant steady-state Raman gain.

Carrier heating also enhances the transient Raman gain coefficient and shifts the gain saturation regime toward higher pump pulse durations. Since semiconductor plasmas exhibit wave and instability phenomena similar to those in gaseous plasmas, they can serve as a compact and convenient substitute. Semiconductors offer advantages such as easier operation, wide tunability of material parameters, and the absence of confinement issues. Therefore, the present study provides a deeper understanding of stimulated scattering mechanisms and their threshold behaviors in laser-induced plasmas.

Acknowledgements

The author sincerely thanks Dr. Manjeet Singh, Assistant Professor, Department of Physics, Government College, Matanhail, Jhajjar – 124106 (Haryana), India, for his valuable suggestions in conducting this research and for meticulously reviewing the manuscript.

References

[1] R.L. Sutherlands, *Handbook of Nonlinear Optics*, Marcel Dekker, New York (2003).
[2] S.I. Anisimov, V.A. Khokhlov, *Instabilities in Laser Matter Interaction*, Academic Press, New York (1995).
[3] K.A. Brueckner, S. Jorna, Laser-driven fusion, *Rev. Mods. Phys.* **46** (1974) 325-367.
[4] C.S. Liu, M.N. Rosenbluth, R.B. White, Raman and Brillouin scattering of electromagnetic waves in inhomogeneous plasmas, *Phys. Fluids* **17** (1974) 1211-1219.
[5] J.F. Drake, P.K. Kaw, Y.C. Lee, G. Schmidt, C.S. Liu, M.N. Rosenbluth, Parametric instabilities of electromagnetic waves in plasmas, *Phys. Fluids* **17** (1974) 778-785.
[6] D.W. Forslund, J.M. Kindel, E.L. Lindman, Nonlinear behaviour of stimulated Brillouin and Raman scattering in laser irradiated plasmas, *Phys. Rev. Lett.* **30** (1973) 739-743.
[7] D.C. Hanna, M.A. Yuratich, D. Cottor, *Nonlinear Optics of Free Atoms and Molecules*, Springer, Berlin (1979), ch. 7.
[8] T.R. Loree, R.C. Sze, D.L. Barker, P.B. Scott, New lines in the UV: SRS of excimer laser wavelengths, *IEEE J. Quantum Electron.* **15** (1979) 337-342.
[9] J.E. Rothenberg, J.F. Young, S.E. Harris, High-resolution extreme ultraviolet spectroscopy of potassium using anti-Stoke's radiation, *Opt. Lett.* **6** (1981) 363-365.
[10] B.Y. Zeldovich, N.F. Pilipetsky, V.V. Shkunov, *Principles of Phase Conjugation*, Springer, Berlin (1985), p. 25.
[11] M.S. Sodha, R.P. Sharma, S.C. Kaushik, Interaction of intense laser beams with plasma waves: stimulated Raman scattering, *J. Appl. Phys.* **47** (1976) 3518-3523.
[12] B. Maraghechi, J.E. Willett, Raman backscattering of electromagnetic extraordinary waves in a magnetized inhomogeneous plasma, *J. Plasma Phys.* **20** (1978) 859-865.
[13] B. Maraghechi, J.E. Willett, Raman backscattering of circularly polarized electromagnetic waves propagating along a magnetic field, *J. Plasma Phys.* **21** (1979) 163-172.
[14] C.H. Lee, *Picosecond Optoelectronic Devices*, Academic Press, New York (1984), pp. 1-9, 119-188, 219-284.
[15] H.N. Gibbs, *Optical Bistability: Controlling Light with Light*, Academic, Orlando (1985).
[16] B.S. Wherrett, *Optical Computing*, SUSSP, Edinburg (1989), pp. 1-21.
[17] Gopal, B.S. Sharma, J. Singh, M. Singh, Steady-state and transient Raman gain coefficients of semiconductor magneto-plasmas (Calculated for n-InSb-CO_2 laser system), *Iran. J. Sci. Technol. Trans. Sci.* **46** (2022) 697-708.
[18] Gopal, B.S. Sharma, J. Singh, M. Singh, Enhanced Raman

gain coefficients of semiconductor magneto-plasmas, *Appl. Phys. A* **128** (2022) 309.
[19] J. Singh, S. Dahiya, M. Singh, Raman amplification in magnetoactive doped III-V semiconductors, *J. Opt*. **51** (2022) 317-326.
[20] J. Singh, S. Dahiya, M. Singh, Enhanced Raman gain coefficients (under steady-state and transient regimes) of semiconductor magneto-plasmas, *Pramana J. Phys*. **95** (2021) 208.
[21] J. Singh, S. Dahiya, M. Singh, Free and bound charge carriers dependent Raman susceptibilities in weakly-polar magnetoactive semiconductors, *Materials Today: Proc*. **46** (2021) 5844-5851.
[22] J. Singh, S. Dahiya, M. Singh, Steady-state and transient Raman gain coefficients of weakly-polar magnetoactive doped semiconductors, *Materials Today: Proc*. **49** (2022) 1189-1195.
[23] J. Singh, S. Dahiya, A. Kumar, M. Singh, Enhanced Raman gain coefficients of semiconductor magneto-plasmas, *Optik* **248** (2021) 168183.
[24] M. Singh, V. Pal Singh, A. Sangwan, P. Aghamkar, D. Joseph, Influence of Szigeti effective charge on coherent Raman scattering of laser radiation in magnetized direct gap semiconductors, *J. Nonlin. Opt. Phys. Mat*. **23** (2014) 1450024.
[25] M.C. Steele, B. Vural, *Wave interactions in Solid State Plasmas*, McGraw Hill, New York (1969), p. 105.
[26] S.D. Kramer, F.G. Parsons, N. Bloembergen, Interference of third-order light mixing and second harmonic exciton generation in CuCl, *Phys. Rev. B* **9** (1974) 1853-1856.
[27] K. Nishikawa, Parametric excitation of coupled waves 1. General Formulation, *Phys Soc Jpn* **24** (1968) 916-922.
[28] M. Singh, P. Aghamkar, Coherent Brillouin scattering in non-centrosymmetric semiconductors: bound and free charge carriers contribution, *J. Mod. Opt*. **55** (2008) 1251-1265.
[29] A.C. Beer, *Galvanometric Effects in Semiconductors: Solid State Physics*, Academic Press, New York (1963).
[30] M.S. Sodha, A.K. Ghatak, V.K. Tripathi, *Self-Focusing of Laser Beams in Dielectrics, Plasmas and Semiconductors*, Tata McGraw, New Delhi (1974), pp. 55-62.
[31] E.M. Conwell, *High Field Transport in Semiconductors*, Academic Press, New York (1967), pp. 159.
[32] J.M. Mayer, F.J. Bartoli, M.R. Kruer, Optical heating in semiconductors, *Phys. Rev. B* **21** (1980) 1559-1568.
[33] M. Kruer, L. Esterowitz, F. Bartoli, R. Allea, *Laser Induced Damage in Optical Materials,* A.J. Glass, A.H. Guenther (Ed.), NBS Special Publication No. 509, Washington (1977), p. 473.
[34] C.S. Wang, *Quantum Electronics*, Academic Press, New York (1975), pp. 447-472.
[35] D. Vonder Linde, A. Laubereau, W. Kaiser, Molecular vibrations in liquids: direct measurement of the molecular dephasing time: determination of the shape of picosecond light pulses, *Phys. Rev. Lett*. **26** (1971) 954-957.